

# Two-phase oil–gas pipe flow imaging by simulated annealing

C Ortiz-Alemán and R Martín

Instituto Mexicano del Petroleo, Eje Central L Cardenas Nte 152, DF, CP 07730, Mexico

Received 26 October 2004

Accepted for publication 25 January 2005

Published DD MMM 2005

Online at [stacks.iop.org/JGE/2/1](http://stacks.iop.org/JGE/2/1)

## Abstract

We introduce a numerically improved image reconstruction technique for imaging two-phase oil–gas pipe flows using electrical capacitance tomography, based on simulated annealing and iterative linear forward modelling. In the simulated annealing method, a permittivity image is reconstructed by minimizing iteratively an energy function related to the difference between the measured ECT data and those calculated for an estimated permittivity distribution. The permittivity model is repeatedly updated, in a semi-random process that mimics the thermodynamic phenomenon of crystallization in a liquid that is being cooled. In this work, the forward problem is calculated by using a numerically optimized linear approach that makes use of the sensitivity matrix which is computed in the beginning of the process and is not subsequently updated. The images are refined as they go through the processes of cooling and random perturbation of model parameters until their calculated capacitance data match the measured data in a least-squares sense. As each new model is roughly the same as the previous one except for one perturbed parameter, the forward problem computation can be accelerated by avoiding redundant operations. We found this technique to be faster and more accurate than traditional linear methods commonly used in the context of this application.

## Abbreviations

ECT	electrical capacitance tomography
FVM	finite volume method
GA	genetic algorithms
LBP	linear back-projection
SA	simulated annealing
VFSA	very fast simulated annealing

## 1. Introduction

Inverting electrical capacitance tomography (ECT) data to reconstruct permittivity distributions flowing through a pipe is a very important topic in oil engineering research. Additionally, ECT has potential applications to imaging, monitoring and controlling numerous industrial multiphase processes. In the last two decades, electrical capacitance tomography (ECT) has been developed intensively for non-intrusive tomography purposes. ECT is a technique which has been preferably chosen among other tomography methods such as ultrasound, optical, x-ray and gamma-ray processes to obtain reconstructed images of multiphase flows in the

inner core or region of a non-conductive body. An extensive review of the different ECT systems, their techniques and applications developed since the 1980s till the beginning of the 1990s has been written in 1992 (Dickin *et al* 1992). The first real-time ECT system has been performed at UMIST at the beginning of the 1990s to visualize two-phase flow systems in pipelines (Huang *et al* 1992, Xie *et al* 1992). In those years and the following, different hardware process systems based on similar concepts have been developed using 4 to 16 electrodes, thanks to the improvement of the electronic transducers (Isaksen and Nordtvedt 1993, Isaksen 1996). Since 1995, the needs of process applications have increased and made possible due to the significant improvement of the design and operation of the process plants equipment (Beck *et al* 1997). More specifically, this non-intrusive technique allows us to determine the permittivity distribution and then the composition of two-phase mixtures like gas–solid or gas–oil systems. It has many useful applications in measurement of multiphase flows for the oil industry and more specifically in the study of oil–gas pipe flows, gas–solid distributions in pneumatic conveyors and fluidized beds, flame combustion processes, water–oil–gas separators and trickle bed reactors

for water content measurements (Yang *et al* 1995a, 1995b, Yang and Peng 2003).

However, so far the main limiting factor to the practical application of ECT has been the lack of fidelity or accuracy of the images obtained using the available image reconstruction methods (Yang and Peng 2003). Simple direct methods such as linear back-projection (LBP) yield relatively poor images that only provide a qualitative indication of the component distribution inside the sensor. On the other hand, more sophisticated methods, based on iterative local optimization techniques, generally require one or more regularization parameters whose optimal value depends precisely on the (unknown) image to be reconstructed, apart from the fact that the regularization employed has the effect of smoothing the image contours, making it more diffuse. These iterative local optimization techniques smooth the whole image in some configurations where sharp permittivity contrasts are present, and do not converge as desired in some cases. This is mainly due to the fact that they perform local searches of the real solution around an initial guess which is not so good, particularly when flows moving with time are considered. Newton–Raphson (Hansen 1998), Landweber (Yang *et al* 1999, Liu *et al* 1999), steepest descent methods as well as the algebraic reconstruction technique, the simultaneous iterative reconstruction technique (Reinecke and Mewes 1996, Su *et al* 2000), and the model based on iterative algorithm (Isaksen and Nordtvedt 1993) define these most common iterative methods. For a too strong regularization, smoothing effects will appear, and for a too slight one, the technique becomes unstable and hardly converges. These problems are due to the fact that the reconstruction is non-linear and the linear algorithms previously mentioned are suitable tools for two-phase flows but hardly apply for complex flows like bubbly or three-phase flows (Yang and Peng 2003). Thus, there is a need of better and more accurate image reconstruction methods.

As the value of the mutual capacitances is a complex non-linear function of the conductor system geometry, and of the spatial distribution of permittivity, such inversion is inherently non-linear. In a previous work (Ortiz-Alemán *et al* 2003), we introduced a global optimization algorithm based on simulated annealing for permittivity image reconstruction from ECT data.

In many geophysical research areas, linear methods such as least-squares, steepest descent or Levenberg–Marquardt algorithms (Li *et al* 2004) and non-linear imaging techniques (Sen and Stoffa 1995) have been tested in order to retrieve physical properties of the geological media under study. Among global optimization techniques, the simulated annealing (SA) method is a non-linear optimization algorithm that has proved to be efficient for many non-linear problems of interest in geophysics (Vasudevan *et al* 1991, Sen and Stoffa 1995); therefore SA is well suited to perform two-phase flow imaging by inversion of both synthetic and measured data (Ortiz-Alemán *et al* 2003, 2004). The simulated annealing method was conceived in close analogy to optimization systems occurring in nature (Kirkpatrick *et al* 1983). It can be seen as an improvement to the famous Monte Carlo method.

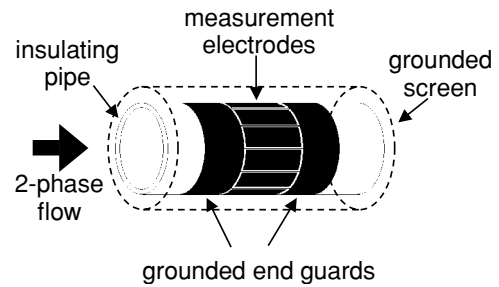


Figure 1. Capacitance tomography sensor.

The SA-based ECT data inversion has some advantages over other approaches: it can find good solutions starting from any initial model, can more easily implement complex *a priori* information, and does not introduce smoothing effects in the final permittivity distribution model. A major disadvantage comes from the fact that SA is computationally intensive and leads to relatively slow reconstructions. In order to optimize the numerical burden of the method, we developed a new hybrid approach combining global inversion by SA and linear forward modelling.

## 2. Linear forward modelling

We used a 12-electrode tomography system (figure 1). The interior of the two-dimensional (2D) sensor was divided into  $p$  regions (or ‘pixels’) where the permittivity was considered as constant, and then the discrete version of the forward problem is

$$\mathbf{c} = \begin{bmatrix} c_1 \\ \vdots \\ c_m \end{bmatrix} = \mathbf{f}(\boldsymbol{\varepsilon}) = \begin{bmatrix} f_1(\boldsymbol{\varepsilon}) \\ \vdots \\ f_m(\boldsymbol{\varepsilon}) \end{bmatrix} \quad \text{with} \quad \boldsymbol{\varepsilon} = \begin{bmatrix} \varepsilon_1 \\ \vdots \\ \varepsilon_p \end{bmatrix} \quad (1)$$

where  $\mathbf{c}$  is the vector of  $m$  possible and independent mutual capacitances (per unit length),  $f_i$  are non-linear functions not known explicitly and  $\boldsymbol{\varepsilon}$  is the vector of permittivity corresponding to the  $p$  regions or pixels within the sensing zone. Applying Gauss’s law (for a 12-electrode system), the mutual capacitances per unit axial electrode length can be calculated as

$$c_k = \frac{q_i}{v_j} = -\frac{\varepsilon_0}{V} \oint_{\Gamma_i} (\boldsymbol{\varepsilon} \nabla \phi^j) \cdot d\mathbf{l} = -\frac{\varepsilon_0}{V} \oint_{\Gamma_i} \boldsymbol{\varepsilon} \frac{\partial \phi^j}{\partial n} dl, \quad k = i + (j - 1) * 12, \quad i \neq j, \quad i, j = 1, \dots, 12 \quad (2)$$

where  $\varepsilon_0$  is the permittivity of free space, equal to  $8.854 \times 10^{-12} \text{ FM}^{-1}$ ,  $\Gamma_i$  is a closed curve surrounding electrode  $i$ ,  $d\mathbf{l}$  is a normal vector representing an element of the curve  $\Gamma_i$ ,  $dl$  is an element of length of that curve, the centre dot represents the scalar product, and  $\phi^j$  is the electrostatic potential produced in the sensor when applying a voltage of  $V$  volts to electrode  $j$  (which is called source or excitation electrode) and 0 V to all others (called detection electrodes).

The potential  $\phi^j$  is determined by the solution of the following partial differential equation

$$\nabla \cdot \boldsymbol{\varepsilon}(x, y) \nabla \phi^j = 0 \quad (3)$$

subject to the boundary conditions (a)  $\phi^j = V$  volts on the

source electrode and (b)  $\phi^j = 0$  on the detection electrodes and the outer screen.

In order to get a linearized version of this forward problem we computed a sensitivity map for each one of the possible electrode pairs, given by

$$s_{ik} = \frac{c_i^k - c_{i(\text{emp})}}{c_{i(\text{full})} - c_{i(\text{emp})}} \quad \text{for } i = 1, \dots, m \quad \text{and} \\ k = 1, \dots, p \quad (4)$$

where  $k$  is the pixel number (from 1 to  $p$ ),  $c_i^k$  is the capacitance measured with electrode pair  $i$  when the area of pixel  $k$  is full of a high-permittivity material while the rest of the sensor is full of a low-permittivity material, whereas  $c_{i(\text{full})}$  and  $c_{i(\text{emp})}$  are the capacitances for electrode pair  $i$  when the sensor is full of high- and low-permittivity material, respectively. In this work these sensitivity maps were calculated by solving numerically equation (3) with the finite volume method (FVM) and applying equation (2). Having determined the sensitivity maps, they can be used for obtaining ECT synthetic data, from any permittivity distribution inside the sensor. For this purpose, the measured capacitance data must first be normalized according to

$$\tilde{c}_i = \frac{c_i - c_{i(\text{emp})}}{c_{i(\text{full})} - c_{i(\text{emp})}} \quad \text{for } i = 1, \dots, m \quad (5)$$

where  $\tilde{c}_i$  is the normalized capacitance for electrode pair  $i$  and  $c_i$  is the actual capacitance measured with that electrode pair.

In this way, the linear forward problem in ECT can be written in matrix form as

$$\tilde{\mathbf{S}}\tilde{\boldsymbol{\varepsilon}} = \tilde{\mathbf{c}}, \quad (6)$$

where  $\tilde{\mathbf{c}}$  is a vector of normalized capacitance data (see equation (5)),  $\tilde{\boldsymbol{\varepsilon}}$  is a vector of normalized model permittivity, and  $\tilde{\mathbf{S}}$  is the normalized sensitivity matrix. Normalization of model permittivity and the sensitivity matrix was performed by using the following expressions:

$$\tilde{\varepsilon}_i = \frac{\varepsilon_i - \varepsilon_{i(\text{emp})}}{\varepsilon_{i(\text{full})} - \varepsilon_{i(\text{emp})}} \quad \text{for } i = 1, \dots, p \\ \tilde{s}_{ik} = \frac{s_{ik}}{\sum_{k=1}^p s_{ik}} \quad \text{for } i = 1, \dots, m \quad \text{and} \\ k = 1, \dots, p. \quad (7)$$

### 3. Inversion by simulated annealing

The SA method is based on an analogy with the thermodynamic process of crystallization. A mineral fluid that cools slowly until it reaches a low-energy state, gives rise to the formation of well-defined crystals. If, in contrast, the substance leaves its thermal equilibrium state with a sudden or partial cooling, the resulting crystal will have many defects, or the substance may even form a ‘glass’, characterized by its meta-stable molecular disorder. This concept is used in the context of optimization methods to recognize potentially useful models or configurations.

The atoms of each molecular configuration are equivalent to the model parameters in the inverse problem (i.e., the permittivity of the various image pixels). The system energy for such configuration is related to the energy function associated with the set of parameters involved in the model.

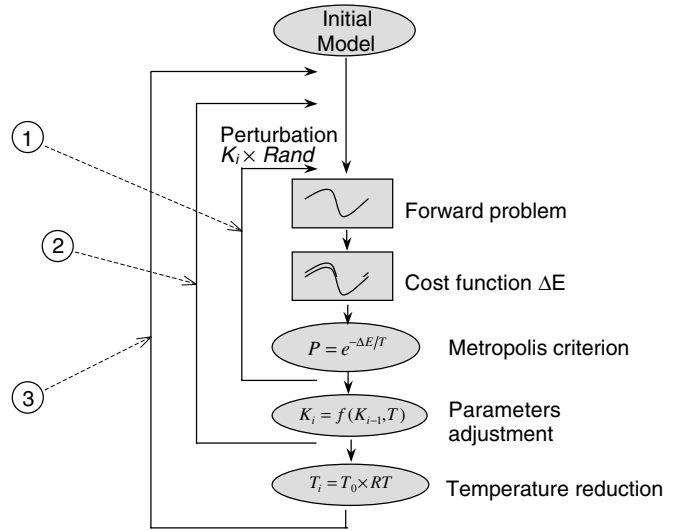


**Figure 2.** Implementation of the SA method (after Ortiz-Aleman *et al* (2004)). The external cycle (3) regulates the system temperature  $T$  (after every cycle is completed) by decreasing  $T$  for each parameter by a factor  $RT$ . The intermediate cycle (2) provides a set of constants  $K_i$  associated with each parameter. This set of constants determines the change applied to each parameter. The inner cycle (1) perturbs the current parameters by multiplying them by their related  $K_i$  constants and random constants lying between  $-1$  and  $1$ . Then, as being discussed in the text, the Metropolis criterion accepts or rejects the new parameters according to a probability function  $P$ .

A least-squares solution can be achieved by minimizing this energy function which is defined as the difference between the observed and synthetic data,

$$E = \frac{\sum_{k=1}^p ((c_{k\text{obs}}) - (c_{k\text{calc}}))^2}{\sum_{k=1}^p (c_{k\text{obs}})^2} \quad (8)$$

where  $p$  is the number of capacitance data,  $c_{k\text{obs}}$  is the  $k$ th observed (measured) capacitance,  $c_{k\text{calc}}$  is the  $k$ th calculated (synthetic) capacitance.

The method of SA has three basic components (Ingber 1989): an energy (or cost, or misfit) function, an order function (the Metropolis criterion), and a set of parameters that control the temperature for each model parameter. The process consists of three nested cycles (figure 2). The external cycle (3) regulates the system temperature. Every time a cycle is completed, the temperature for each parameter decreases as its initial temperature is multiplied by a factor. In this way the desired slow and gradual cooling is carried out. The intermediate cycle (2) generates a set of constants  $K_i$  associated with each parameter. Said constants determine the change that each parameter may experience. In the inner cycle (1), the parameter values are perturbed by multiplying each parameter by the product of its corresponding  $K_i$  times a randomly chosen number between  $-1$  and  $1$ . The synthetic response of the current model is calculated and the change in the system’s energy associated with the new parameter configuration is evaluated. This shift causes a change  $\Delta E$  in the system’s total energy. If  $\Delta E$  is less than or equal to zero, the change in the parameter is accepted and the resulting configuration is considered as the new current configuration. When there is an increase in the system energy ( $\Delta E$  is greater than zero),

the probability  $P$  of acceptance or rejection for the parameter change is determined, according to the Metropolis criterion (Metropolis *et al* 1953), as

$$P(\Delta E) = e^{-\Delta E/T} \quad (9)$$

where  $T$  is the temperature of the system at a given step of the cooling process.

In order to decide whether or not a change that produces an increase in the system's energy is accepted, a random number between 0 and 1 is chosen, which is then compared with the value of the probability corresponding to  $\Delta E$ . If said random number is greater, the parameter shift is not accepted and the configuration that existed before the shift is maintained. Repeating this procedure continuously, the thermal movement of the atoms of a system in thermal equilibrium (at a fixed temperature  $T$ ) is simulated. In order to reach the system's base state, that is to say, the state of lowest energy and highest order, the temperature for each parameter must be reduced very slowly, simulating a quasi-static process. This means that, during the cooling, the system must experience a series of states infinitesimally separated from the state of thermal equilibrium.

The three cycles are repeated, while the temperature of the process decreases progressively. As the temperature diminishes, the parameter variations are smaller and smaller. In this way, the search in the solutions domain tends to confine itself towards the models associated with the global minimum of the energy function.

During the process of reconstructing a permittivity image using SA, it is necessary to solve the forward problem repeatedly for quite similar successive permittivity distributions, while the method converges towards the global solution. Since the solution corresponding to said successive permittivity distributions changes relatively little, it is possible to accelerate the whole process by taking into account the solution corresponding to the previous permittivity configuration. Because this previous guess will be quite close to the next solution, the number of floating-point operations can be dramatically reduced by removing the entire redundant matrix by vector multiplications involved in the computation of the forward problem described by equation (6). To illustrate this numerical improvement of the method, let us consider the case when parameter  $\varepsilon_i$  is being perturbed,

$$\begin{bmatrix} \tilde{s}_{11} & \cdots & \tilde{s}_{1i} & \cdots & \tilde{s}_{1p} \\ \tilde{s}_{21} & \cdots & \tilde{s}_{2i} & \cdots & \tilde{s}_{2p} \\ \vdots & \cdots & \cdots & \ddots & \vdots \\ \tilde{s}_{m1} & \cdots & \tilde{s}_{mi} & \cdots & \tilde{s}_{mp} \end{bmatrix} \begin{bmatrix} \tilde{\varepsilon}_1 \\ \vdots \\ \tilde{\varepsilon}_i + \Delta\tilde{\varepsilon}_i \\ \vdots \\ \tilde{\varepsilon}_p \end{bmatrix} = \begin{bmatrix} \tilde{c}_1 \\ \vdots \\ \vdots \\ \tilde{c}_m \end{bmatrix} \quad (10)$$

where  $\Delta\tilde{\varepsilon}_i$  is the change that parameter  $\varepsilon_i$  may experience in the inner cycle of the SA method. Therefore, computation of a new set of ECT synthetic data can be made by adding a correction factor to the previously computed ECT data vector. That is,

$$\begin{bmatrix} \tilde{c}_1^{\text{new}} \\ \vdots \\ \tilde{c}_m^{\text{new}} \end{bmatrix} = \begin{bmatrix} \tilde{c}_1^{\text{old}} \\ \vdots \\ \tilde{c}_m^{\text{old}} \end{bmatrix} + \Delta\tilde{\varepsilon}_i \begin{bmatrix} \tilde{s}_{1i} \\ \vdots \\ \tilde{s}_{mi} \end{bmatrix}. \quad (11)$$

In this way, a significant amount of floating point operations is saved and computation times are dramatically reduced.

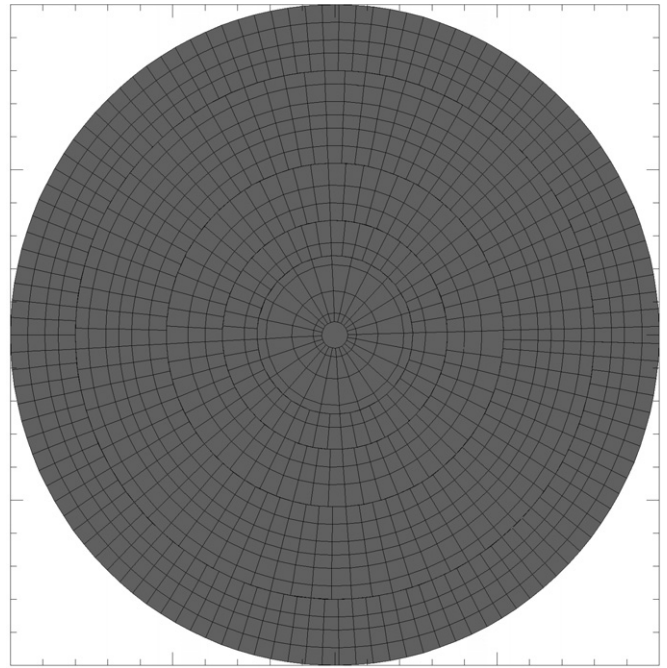


**Figure 3.** Pixel distribution employed in this work for the computation of the sensitivity matrix.

## 4. Results

In a previous work (Ortiz-Aleman *et al* 2004), we followed the advice of Yang and Peng (2003) to test non-linear methods for both forward modelling (FVM) and reconstruction of electrical permittivity images by means of global inversion methods (VFSA). In this paper, we also apply the SA method but we use a linear approximation to the forward problem by means of a numerically improved sensitivity matrix approach. We use a sensitivity matrix computed for a set of 1333 elements or pixels, this pixel distribution is depicted in figure 3.

In the first stage, we applied the SA method to three cases of two-component distributions simulated by placing objects of contrasting permittivity inside the ECT sensor. In figure 4 we summarize the whole set of test cases and their corresponding reconstructed images. In this work we focused our attention on the inversion of measured ECT data as synthetic cases always imply a lower degree of complexity for the SA method (Ortiz-Aleman *et al* 2003, 2004). For comparisons between image reconstruction of synthetic ECT data by the SA method and by other linear approaches, the reader is referred to Ortiz-Aleman *et al* (2004). We stopped the process of inversion of permittivity images at 1 million computations of the forward problem in all these cases. CPU times were quite similar for all cases ( $\sim 22$  s in a 3 GHz Pentium IV PC).

In the first case, we placed a Perspex rod on the left side of the sensor and a nylon rod on the right. We got a reconstructed image with two slightly distorted circular objects located on the right positions and with roughly the same size as the simulated rods. Elongation of the nylon rod and distortion to the right of the Perspex rod are related to the kind of mesh that we employed for the computation of the sensitivity matrix. Another cause for such distortion of the shape is

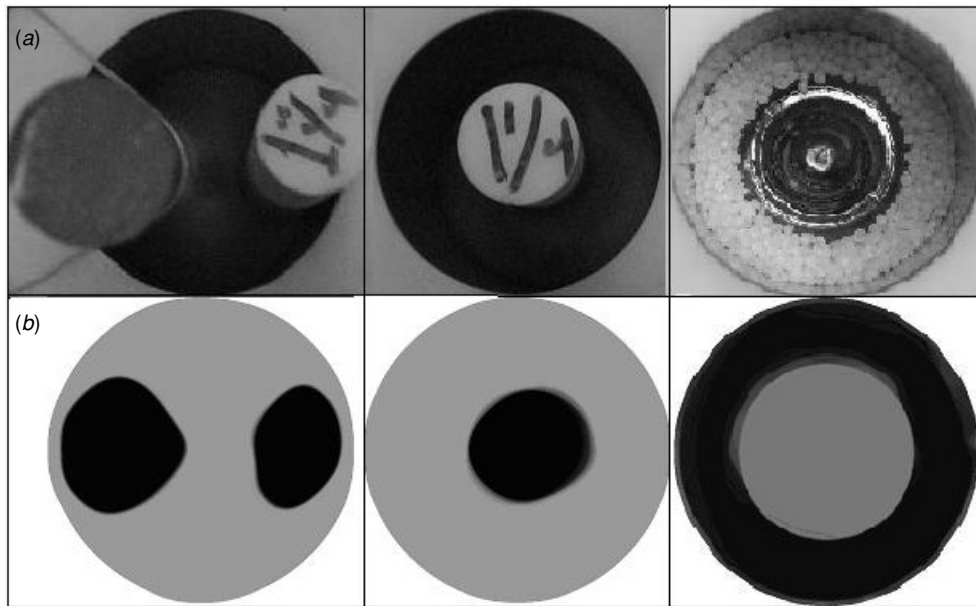


**Figure 4.** Image reconstruction of measured ECT data: (a) test distribution and (b) reconstructed image after 100 000 iterations of the SA method. Black and white represent high- and low-permittivity materials, respectively.

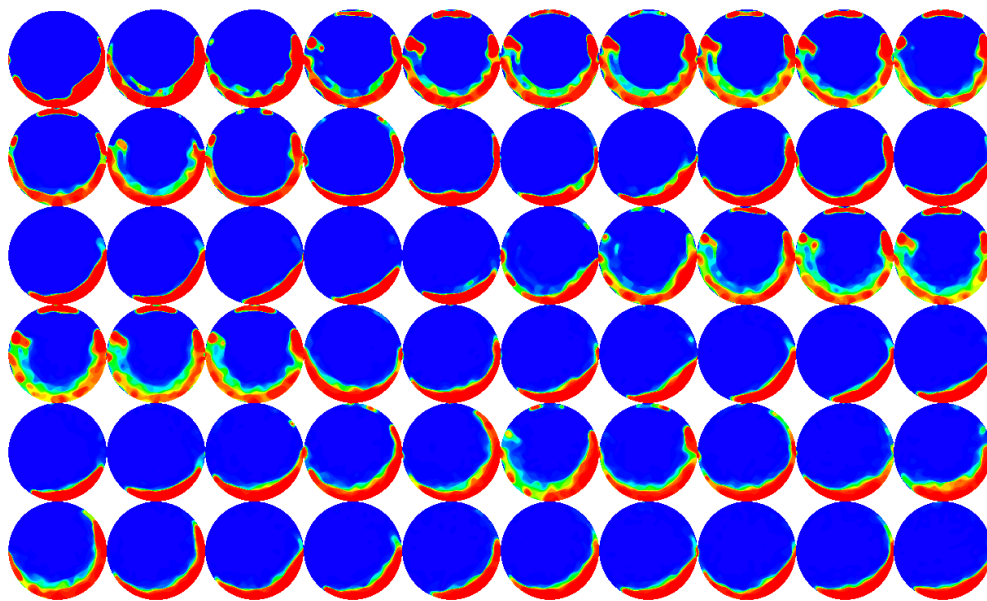


**Figure 5.** Image reconstruction of a real gas–oil two-phase intermittent flow. Red represents high-permittivity material (oil) and blue represents the permittivity of air. Intermediate colours (yellow, green and light blue) are associated with the presence of oil in progressively lower concentrations. Sequence goes from top to bottom and from left to right. Delay time between frames is 50 m.

associated with the process of normalization of the sensitivity and capacitance data. This normalization process tends to guide the search for the optimum model to the close vicinity of the upper and lower bounds of each parameter value. Thus, reconstruction of three different components (two rods with different permittivity values, and air) leads to a distortion of the shape of the object with intermediate permittivity value (the nylon rod located on the right side).

We also studied the case of a nylon rod placed in the centre of the cylindrical sensor. Reconstruction of this second case is also shown in figure 4. The estimated high-permittivity

object is somewhat distorted and slightly shifted to the right.

A third case consisted in locating a plastic bottle with air in the middle of the sensor completely full of polypropylene beads (see figure 4). The reconstructed image reproduces the shape and location of the bottle. Some phantoms of low permittivity value can be seen close to the sensor wall and surrounding the bottle maybe due to the presence of a significant amount of air filling gaps.

In the second stage, we studied the applicability of our SA inversion approach to real data from two-phase oil–gas flows generated in a 3 inch test loop facility. The test loop

uses nitrogen gas, Exxol D80 oil and tap water. In this work, we only used gas and oil as flow components. We used a 12-electrode pressure-resistant capacitance tomography sensor. By varying the oil and gas flow rates, several flow regimes were observed. Gas and oil were injected through the sensor at different pressures up to 7 barg and at a temperature around 20 °C. The velocities of each phase were varied through a pressurized valve system. Ten different flow regimes were generated and sets of measurements during about 30 s were collected for each pattern.

In figure 5 we show a set of results for one of the more complex patterns we found: a stratified-intermittent flow. As can be seen in this plot, large oscillations of the flow are observed in the snapshots, forming semi-annular patterns close to the sensor wall. The liquid flow rate was increased maintaining the gas flow rate low. An intermittent flow pattern is then observed, with an alternate occurrence of slugs and stratified flows. Sequence of reconstructed images goes from top to bottom and from left to right, and delay time between frames is 50 ms.

## 5. Conclusions

Application of linear forward modelling and SA for the inversion of measured ECT data made possible to overcome the major disadvantage of the SA method relative to traditional linear methods: its much higher computation time. As SA requires several thousands of iterations (instead of a few hundreds for linear methods), numerical improvements on the forward problem computation were required in order to significantly reduce its numerical burden.

This hybrid method (linear forward problem and non-linear inverse modelling) does not require a good starting model and is found to be successful in inversion of permittivity images from ECT data. In this paper, the method has been validated by using measured data. The SA method produced satisfactory image reconstructions for all the studied cases. As a consequence of this work, the SA method can be used for routine interpretation of ECT data in two-phase gas–oil flow imaging.

## Acknowledgments

J C Gamio kindly provided measurements of ECT data sets and we thank for his very helpful advice on application of the ECT technology to pipe-flow imaging. This work was supported by projects IMP-D.00117 and IMP-D.00046.

## References

Beck M S, Byars M, Dyakowski T, Waterfall R, He R, Wang S M and Yang W Q 1997 Principles and industrial applications of electrical capacitance tomography *Meas. Control* **30** 197–200

- Dickin F J, Hoyle B S, Hunt A, Huang S M, Ilyas O, Lenn C, Waterfall R C, Williams R A, Xie C G and Beck M S 1992 Tomographic imaging of industrial process equipment—techniques and applications *IEE Proc. G* **139** 72–82
- Hansen P C 1998 *Rank-Deficient and Discrete Ill-Posed Problems* (Philadelphia: SIAM)
- Huang S M, Xie C G, Vasina J, Lenn C, Zhang B F and Beck M S 1992 Experimental evaluation of capacitance tomographic flow imaging system using physical models *Proc. 1st ECAPT Conf. (Manchester 26–29 March) (European Concerted Action on Process Tomography)* ed Beck M S, Campogrande E, Morris M, Williams R A and Waterfall R C (Southampton: Computational Mechanics) pp 361–8
- Ingber L 1989 Very fast simulated re-annealing *Math. Comput. Modelling* **12** 967–3
- Isaksen O 1996 A review of reconstruction techniques for capacitance tomography *Meas. Sci. Technol.* **7** 325–37
- Isaksen O and Nordtvedt J E 1993 A new reconstruction algorithm for process tomography *Meas. Sci. Technol.* **4** 1464–75
- Kirkpatrick S, Gelatt C D and Vecchi M P 1983 Optimization by simulated annealing *Science* **220** 671–80
- Li R, Uren N F, McDonald J A and Urosevic M 2004 Recovery of elastic parameters for a multi-layered transversely isotropic medium *J. Geophys. Eng.* **1** 327–35
- Liu S, Fu L and Yang W Q 1999 Optimization of an iterative image reconstruction algorithm for electrical capacitance tomography *Meas. Sci. Technol.* **10** 37–9
- Metropolis N, Rosenbluth A, Rosenbluth M, Teller A and Teller E 1953 Equation of state calculations by fast computing machines *J. Chem. Phys.* **21** 1087–92
- Ortiz-Aleman C, Martin R and Gamio J C 2003 Application of simulated annealing and genetic algorithms to the reconstruction of electrical permittivity images in capacitance tomography *3rd World Congress on Industrial Process Tomography, (Banff)* (CD Conference Proceedings)
- Ortiz-Aleman C, Martin R and Gamio J C 2004 Reconstructions of permittivity images from capacitance tomography data by using very fast simulated annealing *Meas. Sci. Technol.* **15** 1382–90
- Reinecke N and Mewes D 1996 Recent development and industrial/research applications of capacitance tomography *Meas. Sci. Technol.* **7** 233–46
- Sen M and Stoffa P L 1995 *Global Optimization Methods in Geophysical Inversion* (Amsterdam: Elsevier)
- Su B, Zhang Y, Peng L, Yao D and Zhang B 2000 The use of simultaneous iterative reconstruction technique for electrical capacitance tomography *Chem. Eng. J.* **77** 37–41
- Vasudevan K, Wilson W G and Ladilaw W 1991 simulated annealing static computation using an order-based energy function *Geophysics* **56** 1831–9
- Xie C G, Huang S M, Hoyle B S, Thorn R, Lenn C and Beck M S 1992 Electrical capacitance tomography for flow imaging—system model for development of reconstruction algorithms and design of primary sensors *IEE Proc. G* **139** 89–98
- Yang W Q, Beck M S and Byars M 1995a Electrical capacitance tomography: from design to applications *Meas. Control* **28** 261
- Yang W Q and Peng L 2003 Image reconstruction algorithms for electrical capacitance tomography *Meas. Sci. Technol.* **14** R1–R13
- Yang W Q, Spink D M, York T A and McCann H 1999 An image reconstruction algorithm based on Landweber's iteration method for electrical-capacitance tomography *Meas. Sci. Technol.* **10** 1065–9
- Yang W Q, Stott A L, Beck M S and Xie C G 1995b Development of capacitance tomographic imaging systems for oil pipeline measurements *Rev. Sci. Instrum.* **66** 4326